Metal–Organic Frameworks

DOI: 10.1002/anie.201007277

Nanoscale Light-Harvesting Metal–Organic Frameworks**

*Xuanjun Zhang, Mohamed Ali Ballem, Zhang-Jun Hu, Peder Bergman, and Kajsa Uvdal**

Artificial light-harvesting antenna materials have rapidly gained growing interest in recent years because of their applications in the design of sensors,[1] light-emitting diodes,[2] and solar cells.[3] The long-range ordered organization of donors and acceptors on the nano- to micrometer scale is crucial for efficient Förster resonance energy transfer (FRET) processes in these materials.[4,5] Various elegant strategies have been developed to achieve organized multichromophoric systems, such as organogels[6a] and hybrid hydrogels,[6b] vesicles,[7] and biomolecule-based assemblies.[8,9] Recently, novel approaches to host–guest light-harvesting systems were achieved by loading dye molecules into a single crystal zeolite[10] or periodic mesoporous organosilica.[11] These organizations of dye molecules into long-range ordered solids have proven to be very promising for attaining the desired macroscopic properties. To date, however, the use of nanocrystalline metal-organic frameworks (MOFs) as light-harvesting materials is less explored. MOFs, also known as coordination polymers that are assembled from organic ligands and metal ions, are a very promising type of material with a wide range of potential properties and applications including gas sorption, catalysis, magnetism, fluorescence, and nonlinear optics.[12] Recently, increasing interest has been paid to the miniaturization of MOFs to the nanometer scale; these miniaturized coordination polymers can overcome, to some extent, the limited solution-based behavior of their corresponding bulk materials.[13] The so-called nanoscale coordination polymers[13] have potential applications such as ion exchange,[14] multimodal bioimaging,[15] drug delivery, and sensing.[16] Recent studies showed that some fluorescent molecules confined in coordination polymer nanoparticles by novel adaptive self-assembly or host–guest strategies exhibit remarkably enhanced fluorescence and/or efficient FRET.[17,18] Herein, we envisaged the use of nanoscale metal-organic frameworks (NMOFs) as light harvesting antenna materials because chromophores densely embedded within the frameworks can increase the light absorption cross-section while solution-based behavior of nanocrystals provides potential for further applications.

[*] Dr. X. Zhang, M. A. Ballem, Z.-J. Hu, Prof. Dr. P. Bergman, Prof. Dr. K. Uvdal
Department of Physics, Chemistry, and Biology
Linköping University, 58183 Linköping (Sweden)
Fax: (+46) 13-28-8969
E-mail: kajsa@ifm.liu.se

[**] We acknowledge the support from the Swedish Foundation for Strategic Research (SSF) within the Nano-X program (Grant No. SSF [A3 05:204]) and from VINNOVA with the program Innovations for future health, Multifunctional Nanoprobes for Biomedical Visualization DNr: 2008-03011.

Supporting information for this article is available on the WWW under http://dx.doi.org/10.1002/anie.201007277.

In light-harvesting systems, the energy-transfer efficiency and optical properties always depend on the donor/acceptor ratios. Compared with encapsulation by weak noncovalent interactions, self-assembly by stronger metal–ligand complexation can stabilize different components in the frameworks and decrease the possibility of leakage, which is especially important for sensors beased on FRET.[1] However, the arrangement of different components into long-range ordered frameworks is challenging.[13] Owing to different intermolecular forces in the precursor solution, such as counter ionic interactions, hydrogen bonding, and π–π interactions, coordination polymers easily aggregate to form amorphous particles. Recently, crystalline NMOFs have been prepared by surfactant-assisted processes or by approaches combining surfactants with hydrothermal techniques, microwave, or ultrasonication.[15,19] However, further efforts are needed to remove excess surfactant molecules encapsulated in the porous structure. Herein, we report a surfactant-free method to create highly crystalline NMOFs. Direct functionalization of ligands using long alkyl chains can effectively stabilize lanthanide carboxylate nanocolloids. The affinity of carboxylate groups for lanthanide ions, which have high coordination numbers, is the driving force for the formation of stable three-dimensional networks, while the long alkyl chains in the ligands exclude the aggregation of the final nanoparticles. Different lanthanide ions and energy donors and acceptors can be rapidly organized into ordered frameworks by this coordination-directed assembly process.

Herein, we present a series of different π-conjugated dicarboxylate ligands with differing side-chain lengths (Scheme 1). Nanoparticles derived from these ligands were studied and those prepared from H_2**L1** were chosen as a starting point (Figure 1). Well-defined nanocolloids of coordination polymers were prepared by addition of $[Ln(OAc)_3]$ (Ln = Gd, Eu, Yb) to a DMF solution of H_2**L1** and were left to react at 140 °C for ten minutes. The material is very stably dispersed in DMF; no precipitate was observed after standing of the dispersion at room temperature for six months. Elemental analysis and IR spectra (see Figure S4 in the Supporting Information) reveal that the ligand is deprotonated to form the neutral coordination polymers $Ln_2(\mathbf{L1})_3 \cdot (DMF)_x \cdot (H_2O)_y$ (x, $y = 1$–2), which are in the following abbreviated as Ln–**L1**. SEM and TEM reveal that the particles have discuslike shape with thicker centers and sharp edges. Representative SEM and TEM images of Eu–**L1** nanoparticles are shown in Figure 1a. The discus particles have average diameters of approximately 200–300 nm and center thickness of approximately 30–60 nm. High-resolution TEM (HRTEM) analysis reveals that the discuslike particles exhibit a long-range ordered structure. As shown in Figure 1b, highly ordered nanoscale channels can clearly be seen from the side view of a stand-up Eu–**L1** particle. The

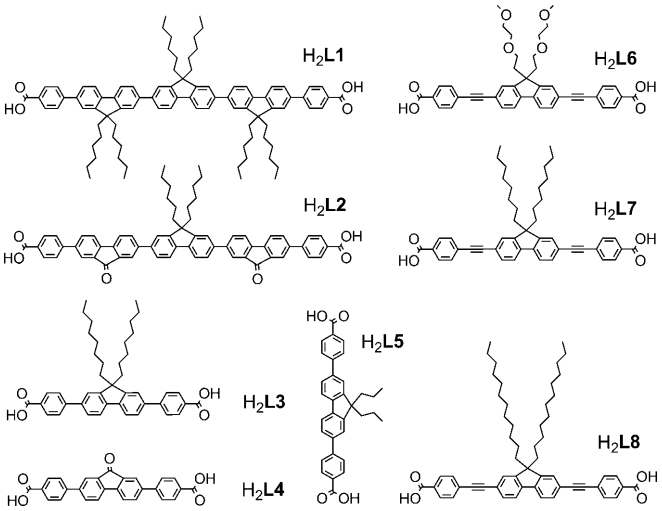

Scheme 1. Chemical structures of the ligands with different π-conjugation lengths and side chains.

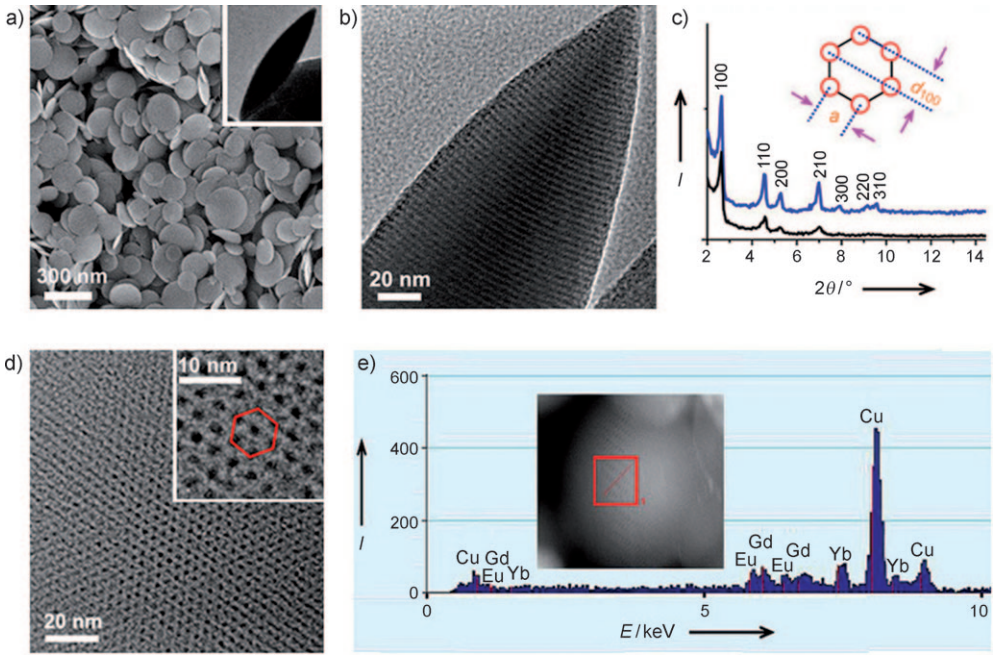

Figure 1. a) SEM and TEM (inset) images of Eu–**L1**. b) HRTEM side view of a representative Eu–**L1** particle showing the ordered nanochannels. c) XRD data of Eu–**L1** (black) and Eu–Gd–Yb–**L1** (blue) nanoparticles. Inset: Schematic illustration showing the relationship between the lattice constant *a* and d_{100} of the hexagonal packed pattern. d) HRTEM image of an Eu–Gd–Yb–**L1** nanoparticle, inset: magnified view of the hexagonal packed pores. e) EDAX data measured by STEM mode. The data is collected from the region marked with a red square.

hexagonally packed pores are visualized directly by HRTEM analysis of a particle lying flat on the copper grid (see Figure S5 in the Supporting Information). The d_{100} spacing of Eu–**L1** measured from HRTEM images is approximately 3.3 nm. To date, although numerous porous coordination polymers have been reported, the direct imaging of the porous structure by HRTEM was only achieved for some very rare examples of MOFs that were prepared by hydrothermal synthesis,[20a,b] or at a surfactant-assisted supercritical condition.[20c] The nanoparticles were further characterized by X-ray diffraction (XRD) analysis (Figure 1c). The sharp diffraction peaks indicate that the as-obtained nanoparticles are highly crystalline. The fine reflexions are attributed to a hexagonal structure.[21] A diagram of standard hexagonal packing is shown in Figure 1c (inset). The d_{100} spacing of Eu–**L1** measured from XRD is consistent with that obtained from the HRTEM image. The influence of ligand structures on the final Ln^{III}–carboxylate nanoparticles was systematically studied. Experimental results reveal that longer alkyl chains (H_2**L3**, H_2**L7**, and H_2**L8**) and more alkyl groups (H_2**L1**) in the ligands make nanoparticles more crystalline and lead to less aggregation (see the Supporting Information).

Different lanthanide ions can be organized by this coordination-directed assembly strategy. The discus morphology does not change when two or three different kinds of metal ions are used as connectors. For example, stable Eu–Gd–Yb–**L1** colloids were obtained by addition of premixed [Ln(OAc)$_3$] (Ln = Eu, Gd, Yb, with molar ratios of 1:1:1) to a DMF solution that contains H_2**L1** at 140 °C. TEM images reveal that the Gd–Eu–Yb–**L1** nanoparticles are relatively uniform with diameters of approximately 200 nm. XRD data reveal that the sample has a highly ordered hexagonal structure (Figure 1c). Seven fine reflexions (*d* spacings: 3.365, 1.948, 1.672, 1.265, 1.121, 0.968, 0.923 nm) correspond to the squared spacing ratios 1, 3, 4, 7, 9, 12, 13, and to the indexing (*hk*) = (10), (11), (20), (21), (30), (22), (31), respectively.[21] HRTEM images are shown in Figure 1d. The distance between two adjacent pore centers is approximately 3.3–3.5 nm, which is comparable to that of Eu–**L1**. The presence of three kinds of lanthanides was confirmed by energy-dispersive analysis of X-rays (EDAX). Figure 1e shows the EDAX data obtained by using STEM mode; the data was collected from the section marked with red color. This result reveals that all three kinds of lanthanides are organized into single nanoparticles. The atomic ratio between the three elements is 8.6:8.0:8.9 based on EDAX result, which roughly is consistent with the feed ratio in the synthesis.

Different ligands can also be organized by this coordination-directed assembly process. Efficient light-harvesting antenna can be achieved by doping the framework of Ln–**L1** nanoparticles with H_2**L2**. Illustrations that show the preparation of the light-harvesting NMOF and an energy

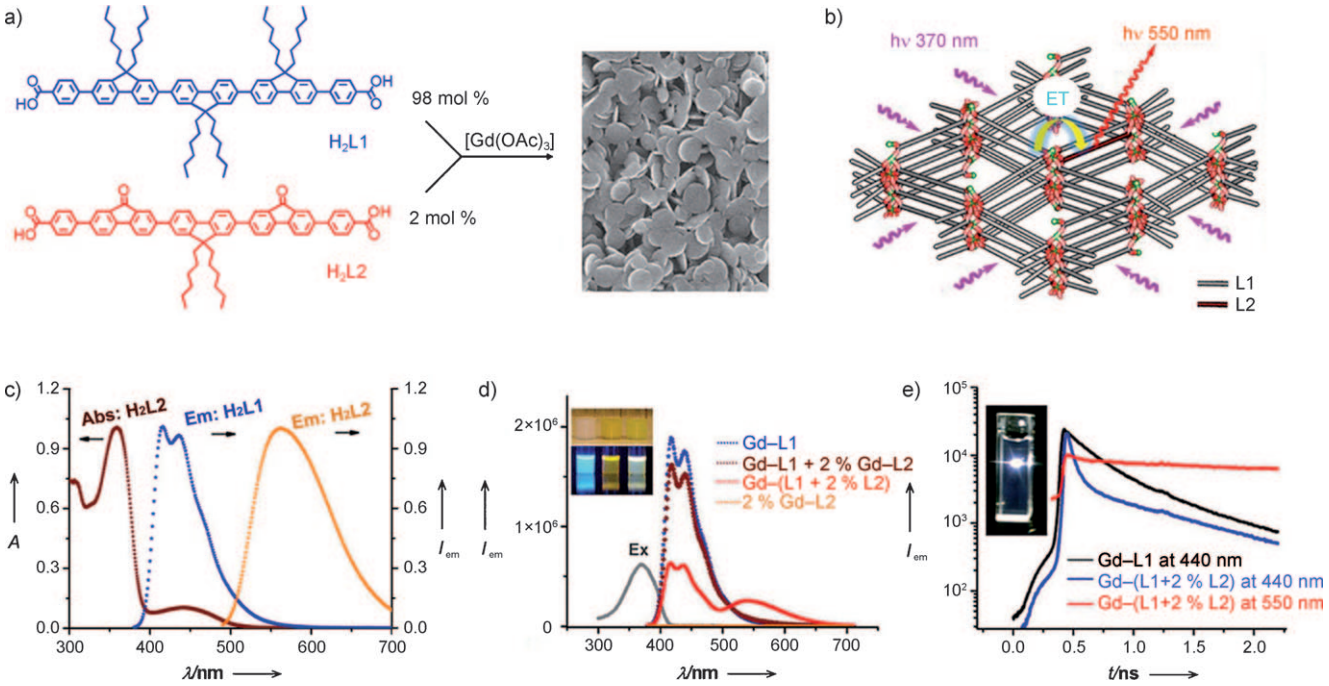

Figure 2. Synthesis and light harvesting study of multicomponent nanoparticles: a) Illustration showing the preparation of Gd–**L1**–**L2** multicomponent nanoparticles. b) Schematic representation of the energy transfer in long-range ordered MOFs. c) Normalized absorption and emission spectra of H_2**L1** and H_2**L2** in DMF. d) Emission spectra of Gd–**L1**, Gd–**L1** mixed with 2 mol% Gd–**L2**, Gd–(**L1** + 2 mol% **L2**), and Gd–**L2** nanoparticles. The gray curve is the excitation spectrum of Gd–(**L1** + 2 mol% **L2**) nanoparticles; inset (from left to right): photoimages of Gd–**L1**, Gd–**L2**, and Gd–**L1**–**L2** nanoparticles in daylight (upper row) and under an ultraviolet lamp (365 nm; bottom row). e) Time-resolved fluorescence decay of Gd–**L1**, Gd–**L2**, and Gd–(**L1** + 2 mol% **L2**). Inset: photoimage of Gd–(**L1** + 2 mol% **L2**) nanoparticles under excitation by laser (370 nm).

transfer (ET) scheme are shown in Figure 2a,b. Our strategy is based on the following factors: firstly, the fluorescence spectrum of H_2**L1** and the S1 absorption band of H_2**L2** overlap well, which favors the Förster-type energy transfer[5–11] between them (Figure 2c); secondly, H_2**L1** and H_2**L2** have the same molecular lengths (ca. 3.5 nm), hence the molecular ordering is not seriously influenced when small amounts of **L2** are added to Ln–**L1** frameworks. To rule out the emission from Eu^{III} and Yb^{III}, we use Gd^{III} as connector to fabricate light-harvesting nanoparticles.

Stable colloids were obtained by addition of [Gd-$(OAc)_3{\cdot}4H_2O$] to a DMF solution that contains H_2**L1** premixed with H_2**L2** (2 mol%) at 140 °C. Nanoparticles with different H_2**L2** doping concentrations were also investigated. The particles kept the discus-like morphology and smooth surface even if the MOF was doped with 5 mol% of H_2**L2**, as revealed by SEM measurements (see Figure S6 in the Supporting Information). In the absence of [$Gd(OAc)_3$], the strong fluorescence of H_2**L1** (1×10^{-6} M in DMF) was not even quenched after addition of 10 mol% of H_2**L2** (see Figure S7 in the Supporting Information). In contrast, efficient light harvesting was observed for Gd–**L1** nanoparticles with 2 mol% of **L2** in the frameworks. When the multicomponent nanoparticles are excited at 360 nm (the absorption maximum of donor **L1**), apparent quenching could be seen for the strong emission of Gd–**L1** ($\Phi = 0.78$), and the concomitant increase in the acceptor emission reached a maximum at about 550 nm (Figure 2d), thus indicating excitation energy transfer from **L1** to **L2**. The multicomponent Gd–**L1**–**L2** nanoparticles exhibit bright white emission (Figure 2d) as the emission covers most of the visible region (overall $\Phi = 0.31$).

The energy transfer is supported by the excitation spectrum of Gd–**L1**–**L2** nanoparticles dispersed in DMF. As shown in Figure 2d, there is only one band at around 370 nm in the excitation spectrum, which indicates that the long-wavelength emission band comes from energy transfer rather than direct excitation of the H_2**L2** at 440 nm. Although H_2**L2** ($\Phi = 0.08$) has an additional absorption band at about 360 nm, the emission from direct excitation of **L2** at 360 nm is negligible (Figure 2d, orange curve) because the final concentration of **L2** for the measurement in Gd–**L1**–**L2** nanoparticles is very low (2×10^{-8} M). A comparison experiment was carried out, in which the ester of **L2** (compound **3** in Scheme S1 in the Supporting Information) was used as acceptor instead of H_2**L2**. Experimental results showed that there is no efficient FRET observed although ester **3** has similar absorbance and emission properties; because of the lack of carboxylate groups, ester **3** cannot be assembled into the framework by a coordination-directed process. The tunable emission might also result from physically mixed Gd–**L1** and Gd–**L2** nanoparticles. To rule out this possibility, another comparison experiment was carried out by mixing Gd–**L1** and 2 mol% Gd–**L2** nanoparticles (based on ligand concentrations). As shown in Figure 2d (brown curve), a slight decrease of the emission intensity of Gd–**L1** occurred after addition of 2 mol% Gd–**L2,** but no apparent energy transfer emission was observed. These results indicate that organization of the donor and the acceptor into long-range

ordered structures can effectively promote the energy migration. Time-resolved fluorescence decay of Gd–**L1** nanoparticles dispersed in DMF (Figure 2e) is 0.79 ns. This lifetime is shortened to 0.33 ns by doping of H_2**L2**, accompanied by a fast rise in the decay profile of **L2** emission. The lifetime of energy transfer emission in Gd–**L1**–**L2** nanoparticles detected at 550 nm is longer (5.06 ns) compared to free H_2**L2** (4.79 ns). These results again indicate energy transfer from **L1** to **L2** within the frameworks.

We also show herein another kind of light-harvesting antenna, in which the acceptor ligand (H_2**L4**) and Eu^{III} in multicomponent nanoparticles can be co-sensitized by the same donor H_2**L3** (Figure 3). Coordination-directed assembly of Gd^{III} and H_2**L3** with 1% mol of H_2**L4** doping results in an efficient light harvesting (Figure 3b). The FRET process is

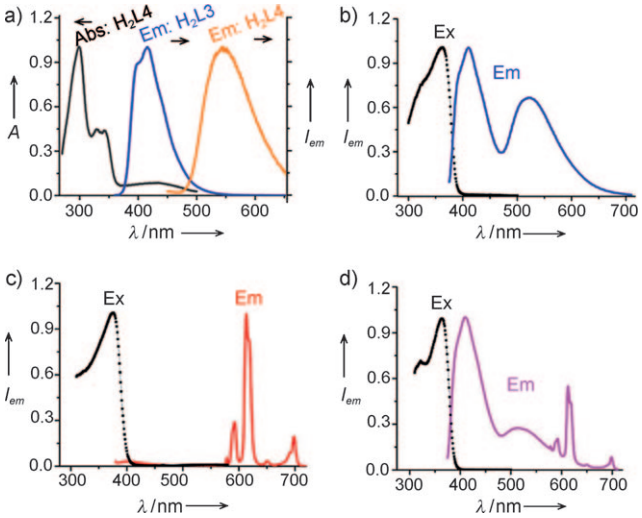

Figure 3. a) Normalized UV/Vis absorption and emission spectra of H_2**L3** and H_2**L4** in DMF. b) Excitation and emission spectra of Gd–(**L3** + 1% mol **L4**) nanoparticles. c) Excitation and emission spectra of Eu–**L3** nanoparticles. d) Excitation (detected at 590 nm) and emission spectra of $Gd^{III}_{0.95}$–$Eu^{III}_{0.05}$–$\mathbf{L3}_{1.47}$–$\mathbf{L4}_{0.03}$ multicomponent nanoparticles dispersed in DMF.

very similar to that of the Gd–**L1**–**L2** system. Interestingly, very efficient sensitization of Eu^{III} is also observed in Eu–**L3** nanoparticles. After coordination with Eu^{III}, the strong emission of H_2**L3** is quenched and red emission of Eu^{III} is sensitized (Figure 3c). These interesting results inspired us to investigate the optical properties of multicomponent nanoparticles. Figure 3d showed the excitation and emission spectra of $Gd^{III}_{0.95}$–$Eu^{III}_{0.05}$–$\mathbf{L3}_{1.47}$–$\mathbf{L4}_{0.03}$ nanoparticles. The multiband emissions (with bands at 420, 530, and 612 nm) cover the entire visible region, although the intensities are not well balanced. Excitation spectra monitored at different emission wavelengths from 390 to 700 nm exhibit very similar characteristics to those shown in Figure 3b and c, indicative of co-sensitization of both **L4** and Eu^{III} by the same donor **L3**. The multiband emissions from these multicomponent nanoparticles could potentially be applied as barcodes[22] and sensors based on FRET. To the best of our knowledge, this is the first example of co-sensitization of both the organic acceptor and the metal ion by the same donor in NMOFs.

In conclusion, we have demonstrated a surfactant-free method to create highly crystalline MOF nanoparticles with efficient light-harvesting properties. Direct modification of the ligands by using hydrophobic alkyl chains has been proven to effectively stabilize the particles. Different metal ions, donors, and acceptors have been incorporated into the frameworks by one-step coordination-directed assembly. Experimental results clearly show that the optical properties of NMOFs can be enhanced and tuned by chemical manipulation of the inorganic and organic components in the frameworks. The nanocolloids can form stable dispersions that are not disassembled by common organic solvents and thus provide the possibility of spincoating for further applications. This strategy may encourage efforts toward multicomponent photofunctional nanomaterials.

Experimental Section

Ligand H_2**L1** was synthesized by a previously reported method.[18b] The synthesis of the ligands H_2**L2**–H_2**L8** is described in the Supporting Information. Synthesis of Eu–**L1** nanoparticles: H_2**L1** (0.06 mmol) was dissolved in DMF (25 mL) and heated to 140 °C. A [Eu-$(OAc)_3{\cdot}xH_2O$] (0.04 mmol) solution in DMF (10 mL) was added dropwise under stirring. The white colloids were stirred for 10 min and were left to cool to room temperature. The nanoparticles for the measurements were collected by centrifugation after addition of ethanol/water (25 mL, 1:1), were washed thoroughly with ethanol and dried in vacuum. Elemental analysis calcd (%) for [Eu–$\mathbf{L1}_{1.5}{\cdot}(DMF)_{1.1}{\cdot}(H_2O)_{1.7}$]: C 77.5, H 7.9, N 0.7; found (%): C 77.7, H 8.0, N 0.8. Other nanoparticles such as Gd–**L1** and Yb–**L1** were synthesized by the same method using [$Gd(OAc)_3{\cdot}xH_2O$] or [Yb-$(OAc)_3{\cdot}xH_2O$] instead of [$Eu(OAc)_3{\cdot}xH_2O$]. For the synthesis of multicomponent nanoparticles such as Eu–Gd–Yb–**L1**, Gd–**L1**–**L2**, and Gd–Eu–**L3**–**L4**, premixed ligands and/or [$Ln(OAc)_3$] (Ln = Gd, Eu, Yb) with appropriate molar ratios were used instead of a single ligand or lanthanide acetate.

UV/Vis absorption spectra were collected on a UV-2450 UV/Vis/NIR spectrophotometer. Fluorescence measurements were performed with a Fluoromax-4 spectrofluorometer at room temperature. The quantum efficiency (Φ_{fl}) of the ligands and nanoparticles in dilute DMF solution was measured using quinine sulfate in 0.1 mol L^{-1} sulfuric acid and Coumarin-102 in ethanol as standards. Elemental analysis was performed using a flash 2000 series CHN analyzer. IR spectra were collected on a Bruker vector 33 Fourier transform infrared spectrophotometer (using KBr pellets) in the range 400–4000 cm^{-1}. X-ray diffraction (XRD) measurements of the nanoparticles were performed using powdered samples on a Philips PW 1729 powder X-ray diffractometer ($Cu_{K\alpha}$ radiation) over 2θ ranges from 0.8° to 10° and the data from 2° to 14° were shown in Figure 1e. SEM images were taken on a LEO 1550 FEG scanning electron microscope. TEM and EDX analysis were performed with a FEI Tecnai G2 microscope. The time-resolved fluorescence decay (measured in DMF medium) was investigated by using 370 nm picosecond laser excitation and was detected with a 0.5 m spectrometer equipped with a Synchroscan streak camera. The time resolution is determined by the dispersion in the spectrometer and is typically 20 ps.

Received: November 19, 2010
Revised: March 9, 2011
Published online: May 9, 2011

Keywords: lanthanides · light harvesting · metal-organic frameworks · nanocolloids · nanostructures

[1] a) X. Zhang, S. Rehm, M. M. Safont-Sempere, F. Würthner, *Nat. Chem.* **2009**, *1*, 623 – 629; b) C. Wu, B. Bull, K. Christensen, J. McNeill, *Angew. Chem.* **2009**, *121*, 2779 – 2783; *Angew. Chem. Int. Ed.* **2009**, *48*, 2741 – 2745.

[2] Y. Sun, N. C. Giebink, H. Kanno, B. Ma, M. E. Thompson, S. R. Forrest, *Nature* **2006**, *440*, 908 – 912.

[3] W.-Y. Wong, C.-L. Ho, *Acc. Chem. Res.* **2010**, *43*, 1246 – 1256.

[4] M. R. Wasielewski, *Acc. Chem. Res.* **2009**, *42*, 1910 – 1921.

[5] a) A. D. Elder, A. Domin, G. S. Kaminski Schierle, C. Lindon, J. Pines, A. Esposito, C. F. Kaminski, *J. R. Soc. Interface* **2009**, *6*, S59 – S81; b) O. Bossart, L. De Cola, S. Welter, G. Calzaferri, *Chem. Eur. J.* **2004**, *10*, 5771 – 5775.

[6] a) A. Ajayaghosh, V. K. Praveen, *Acc. Chem. Res.* **2007**, *40*, 644 – 656; b) K. V. Rao, K. K. R. Datta, M. Eswaramoorthy, S. J. George, *Angew. Chem.* **2011**, *123*, 1211 – 1216; *Angew. Chem. Int. Ed.* **2011**, *50*, 1179 – 1184.

[7] F. J. M. Hoeben, I. O. Shklyarevskiy, M. J. Pouderoijen, H. Engelkamp, A. P. H. J. Schenning, P. C. M. Christianen, J. C. Maan, E. W. Meijer, *Angew. Chem.* **2006**, *118*, 1254 – 1258; *Angew. Chem. Int. Ed.* **2006**, *45*, 1232 – 1236.

[8] Y. Ner, J. G. Grote, J. A. Stuart, G. A. Sotzing, *Angew. Chem.* **2009**, *121*, 5236 – 5240; *Angew. Chem. Int. Ed.* **2009**, *48*, 5134 – 5138.

[9] Y. S. Nam, T. Shin, H. Park, A. P. Magyar, K. Choi, G. Fantner, K. A. Nelson, A. M. Belcher, *J. Am. Chem. Soc.* **2010**, *132*, 1462 – 1463.

[10] a) G. Calzaferri, S. Huber, H. Maas, C. Minkowski, *Angew. Chem.* **2003**, *115*, 3860 – 3888; *Angew. Chem. Int. Ed.* **2003**, *42*, 3732 – 3758; b) Y. Wang, H. Li, Y. Feng, H. Zhang, G. Calzaferri, T. Ren, *Angew. Chem.* **2010**, *122*, 1476 – 1480; *Angew. Chem. Int. Ed.* **2010**, *49*, 1434 – 1438.

[11] S. Inagaki, O. Ohtani, Y. Goto, K. Okamoto, M. Ikai, K. Yamanaka, T. Tani, T. Okada, *Angew. Chem.* **2009**, *121*, 4102 – 4106; *Angew. Chem. Int. Ed.* **2009**, *48*, 4042 – 4046.

[12] G. Férey, *Chem. Soc. Rev.* **2008**, *37*, 191 – 214.

[13] For recent reviews, see: a) W. Lin, W. J. Rieter, K. M. L. Taylor, *Angew. Chem.* **2009**, *121*, 660 – 668; *Angew. Chem. Int. Ed.* **2009**, *48*, 650 – 658; b) A. M. Spokoyny, D. Kim, A. Sumrein, C. A. Mirkin, *Chem. Soc. Rev.* **2009**, *38*, 1218 – 1227; c) X. Wang, R. McHale, *Macromol. Rapid Commun.* **2010**, *31*, 331 – 350; d) J. K.-H. Hui, M. J. MacLachlan, *Coord. Chem. Rev.* **2010**, *254*, 2363 – 2390; e) A. Carné, C. Carbonell, I. Imaz, D. Maspoch, *Chem. Soc. Rev.* **2011**, *40*, 291 – 305.

[14] a) M. Oh, C. A. Mirkin, *Nature* **2005**, *438*, 651 – 654; b) M. Oh, C. A. Mirkin, *Angew. Chem.* **2006**, *118*, 5618 – 5620; *Angew. Chem. Int. Ed.* **2006**, *45*, 5492 – 5494.

[15] a) K. M. L. Taylor, W. J. Rieter, W. Lin, *J. Am. Chem. Soc.* **2008**, *130*, 14358 – 14359; b) W. J. Rieter, K. M. L. Taylor, H. An, W. Lin, W. Lin, *J. Am. Chem. Soc.* **2006**, *128*, 9024 – 9025; c) K. M. L. Taylor, A. Jin, W. Lin, *Angew. Chem.* **2008**, *120*, 7836 – 7839; *Angew. Chem. Int. Ed.* **2008**, *47*, 7722 – 7725; d) K. E. deKrafft, Z. Xie, G. Cao, S. Tran, L. Ma, O. Z. Zhou, W. Lin, *Angew. Chem.* **2009**, *121*, 10085 – 10088; *Angew. Chem. Int. Ed.* **2009**, *48*, 9901 – 9904.

[16] a) W. J. Rieter, K. M. Pott, K. M. L. Taylor, W. Lin, *J. Am. Chem. Soc.* **2008**, *130*, 11584 – 11585; b) W. J. Rieter, K. M. L. Taylor, W. Lin, *J. Am. Chem. Soc.* **2007**, *129*, 9852 – 9853; c) K. M. L. Taylor-Pashow, J. D. Rocca, Z. Xie, S. Tran, W. Lin, *J. Am. Chem. Soc.* **2009**, *131*, 14261 – 14263.

[17] a) R. Nishiyabu, C. Aimé, R. Gondo, T. Noguchi, N. Kimizuka, *Angew. Chem.* **2009**, *121*, 9629 – 9632; *Angew. Chem. Int. Ed.* **2009**, *48*, 9465 – 9468; b) C. Aime, R. Nishiyabu, R. Gondo, K. Kaneko, N. Kimizuka, *Chem. Commun.* **2008**, 6534 – 6536; c) C. Aimé, R. Nishiyabu, R. Gondo, N. Kimizuka, *Chem. Eur. J.* **2010**, *16*, 3604 – 3607; d) R. Nishiyabu, C. Aime, R. Gondo, K. Kaneko, N. Kimizuka, *Chem. Commun.* **2010**, *46*, 4333 – 4335.

[18] a) X. Zhang, M. A. Ballem, M. Ahrén, A. Suska, P. Bergman, K. Uvdal, *J. Am. Chem. Soc.* **2010**, *132*, 10391 – 10397; b) X. Zhang, Z.-K. Chen, K. P. Loh, *J. Am. Chem. Soc.* **2009**, *131*, 7210 – 7211.

[19] a) D. Tanaka, A. Henke, K. Albrecht, M. Moeller, K. Nakagawa, S. Kitagawa, J. Groll, *Nat. Chem.* **2010**, *2*, 410 – 416; b) G. Liang, J. Xu, X. Wang, *J. Am. Chem. Soc.* **2009**, *131*, 5378 – 5379; c) Z. Ni, R. I. Masel, *J. Am. Chem. Soc.* **2006**, *128*, 12394 – 12395; d) Z. Q. Li, L.-G. Qiu, T. Xu, Y. Wu, W. Wang, Z.-Y. Wu, X. Jiang, *Mater. Lett.* **2009**, *63*, 78 – 80; e) R. McHale, N. Ghasdian, Y. Liu, H. Wang, Y. Miao, X. Wang, *Macromol. Rapid Commun.* **2010**, *31*, 856 – 860; f) M. Ma, D. Zacher, X. Zhang, R. A. Fischer, N. Metzler-Nolte, *Cryst. Growth Des.* **2011**, *11*, 185 – 189.

[20] a) O. I. Lebedev, F. Millange, C. Serre, G. Van Tendeloo, G. Férey, *Chem. Mater.* **2005**, *17*, 6525 – 6527; b) A. Sonnauer, F. Hoffmann, M. Fröba, L. Kienle, V. Duppel, M. Thommes, C. Serre, G. Férey, N. Stock, *Angew. Chem.* **2009**, *121*, 3849 – 3852; *Angew. Chem. Int. Ed.* **2009**, *48*, 3791 – 3794; c) Y. Zhao, J. Zhang, B. Han, J. Song, J. Li, Q. Wang, *Angew. Chem.* **2011**, *123*, 662 – 665; *Angew. Chem. Int. Ed.* **2011**, *50*, 636 – 639.

[21] E. Terazzi, J. M. Bénech, J. P. Rivera, G. Bernardinelli, B. Donnio, D. Guillon, C. Piguet, *Dalton Trans.* **2003**, 769 – 772.

[22] K. A. White, D. A. Chengelis, K. A. Gogick, J. Stehman, N. L. Rosi, S. Petoud, *J. Am. Chem. Soc.* **2009**, *131*, 18069 – 18071.

